Self-Excited Motions of Volatile Drops on Swellable Sheets

Aditi Chakrabarti,[1] Gary P. T. Choi,[1] and L. Mahadevan[1,2,*]
[1]John A. Paulson School of Engineering and Applied Sciences, Harvard University, Cambridge, Massachusetts 02138, USA
[2]Department of Physics, Harvard University, Cambridge, Massachusetts 02138, USA

(Received 29 September 2019; revised manuscript received 1 February 2020; accepted 22 May 2020; published 25 June 2020)

When a volatile droplet is deposited on a floating swellable sheet, it becomes asymmetric, lobed and mobile. We describe and quantify this phenomena that involves nonequilibrium swelling, evaporation and motion, working together to realize a self-excitable spatially extended oscillator. Solvent penetration causes the film to swell locally and eventually buckle, changing its shape and the drop responds by moving. Simultaneously, solvent evaporation from the swollen film causes it to regain its shape once the droplet has moved away. The process repeats and leads to complex pulsatile spinning and/or sliding movements. We use a one-dimensional experiment to highlight the slow swelling of and evaporation from the film and the fast motion of the drop, a characteristic of excitable systems. Finally, we provide a phase diagram for droplet excitability as a function of drop size and film thickness and scaling laws for the motion of the droplet.

DOI: 10.1103/PhysRevLett.124.258002

When a liquid drop is placed on a rigid substrate, it can either spread or round up depending on the relative magnitude of the surface energies in question. In the presence of an external gradient, the drop can move or evaporate leading to a range of dynamical phenomena that continue to enthrall and instruct, while suggesting a range of applications [1–8]. But could a drop placed on a substrate spontaneously create and respond to gradients by itself?

Our starting point is a volatile liquid droplet of acetone (volume ranging from 1–40 μl) placed on a thin permeable membrane (thickness $H \sim 10$–50 μm), of cross-linked polydimethylsiloxane (PDMS, Sylgard 184, 10∶1) floating on aqueous glycerol [Fig. 1(a)] in ambient conditions. The liquid initially forms a spherical cap on the film [Fig. 1(a)], but within a few seconds, the droplet spontaneously breaks symmetry, first becoming symmetrically lobed, then chirally lobed, and finally beginning to spin [Fig. 1(b) and [9], Movie 1]. The number of lobes is a function of the drop size for a given film thickness; bigger drops have more lobes [Fig. 1(c) and [9], Movie 1]. While there is no preferred chirality, the lobes are equally probable to curve towards a clockwise or anticlockwise direction, and once it is chosen, the drop continues to spin in the same direction; however as it evaporates and becomes smaller, below a threshold size, it eventually stops. If the drop is sufficiently large, it does not spin and instead become polarized, taking the form of a kidney bean or keratocyte [15] and can either oscillate back and forth [Fig. 1(d) and [9], Movie 2] or migrate in a random direction ([9], Movie 3). High speed videos of the motion of the droplets show that in some cases the drop spins smoothly, whereas in other cases it exhibits a pulsatile motion that is limited to the neighborhood of the contact line ([9], Movie 4).

Hypotheses for the undulation and motion include evaporation-driven contact line instability [16] or surface tension-gradient induced Marangoni effects. Replacing acetone by other volatile liquids such as isopropanol and butanol leads to similar phenomena for the film thicknesses $H \sim 10$–50 μm [9]. However, methanol droplets deposited on the same membrane remain stationary while adopting a spherical cap shape, and hexane droplets cause the film to wrinkle but again with no accompanying motion [9]. Since the droplets are composed of one solvent only, we do not expect any compositional Marangoni forces to arise. Furthermore, infrared movies ([9], Movies 6–7) helped us estimate the thermal Marangoni numbers (Ma $\gg 1$, see [9] for details) for the solvents used. While only acetone, isopropanol and butanol show the instability and the other liquids despite having a large thermal Marangoni number do not demonstrate the instability point to the fact that surface tension gradients are not sufficient to create the undulation and motion.

This leaves swelling-induced film deformation and the accompanying droplet motion as the most probable candidate to explain the phenomenon at hand. To quantify this, we first note that the solvent diffuses through the elastic network [17,18] at a rate $kE/\eta aH$, where k is the permeability of drained PDMS network, E is its Young's modulus, η is the dynamic viscosity of the solvent and a is the drop size. Simultaneously, the imbibed solvent leaves the film via a rate of $J/\varepsilon_b H$, where J is its evaporative flux and $\varepsilon_b \sim H/a$ is the strain associated with the fraction of the swollen film that is also responsible for film buckling. If swelling is too fast or too slow relative to evaporation, the result would be a progression towards a (nonequilibrium) steady state. However, if the two processes are in

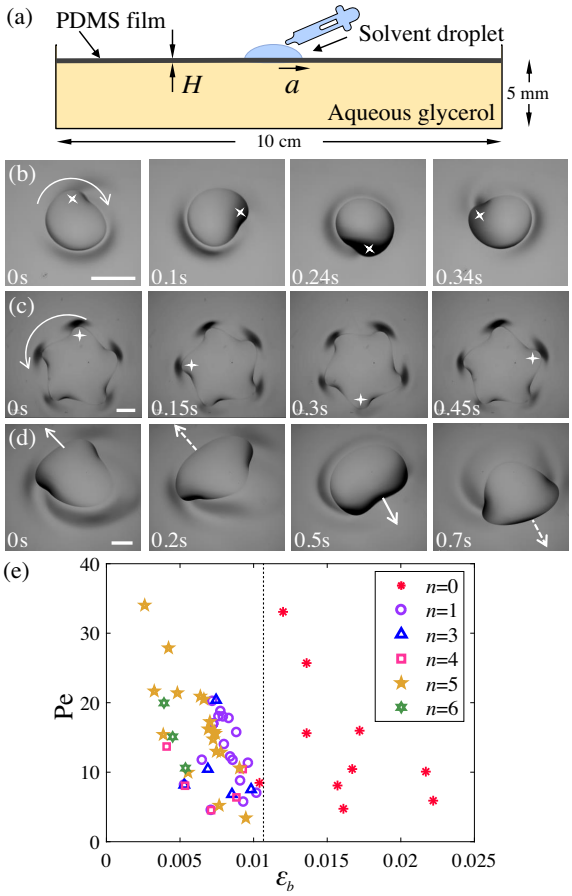

FIG. 1. (a) The experimental setup comprises of a thin elastic film ($H \sim$ tens of microns) made of PDMS afloat aqueous glycerol. Acetone droplets undergo spontaneous rotation as demonstrated via a single cycle of (b) a bean mode with $n = 1$ undergoing clockwise rotation (3 μl drop on 9 μm PDMS film) and (c) a star shaped mode with $n = 5$ undergoing anticlockwise rotation (20 μl drop on 19.5 μm PDMS film), and (d) a 30 μl drop of acetone undergoing oscillatory to and fro motion on a 28.5 μm PDMS film. The scale bars in (b)–(d) denote 2 mm. (e) Peclet numbers [Pe $\sim\mathcal{O}(10)$] plotted as a function of buckling strain (ε_b) for acetone droplets showing droplet instability. The dotted line indicates the critical value of ε_b, which demarcates between spherical cap states ($n = 0$) and lobed states ($n = 1$, 3, 4, 5, 6).

competition, as quantified in terms of the Péclet number Pe$\sim\eta Ja^2/kEH$, one can expect interesting dynamics. Estimating Pe for all solvents tested for given film thicknesses show that acetone, butanol and isopropanol form lobes when Pe$\sim\mathcal{O}(10)$ whereas droplets of methanol and ethanol [Pe$< \mathcal{O}(10)$] as well as hexane and chloroform [Pe $> \mathcal{O}(10)$] do not show the instability [9]. Consistent with these arguments, in environments of saturated solvent vapors, we do not observe drop oscillation or rotation, but droplet spinning resumes when vapor pressure is decreased back to ambient conditions [9].

In this sweet spot that balances evaporation, swelling and hydrodynamics, solvent imbibition in the vicinity of the drop causes the thin film ($H \sim$ tens of microns) to swell and sag to form a dimple that traps the drop ([9], Movie 5), as seen in Fig. 1(b). If the swelling degree is too small (e.g., for a methanol droplet) no lobes form; if the swelling degree is too large (e.g., for a hexane droplet) many wrinkles form. This suggests a simple explanation for the undulation instability of the drops. An elastic strain incompatibility along the nominally circular rim of the swollen film (the region inside is swollen, while the region outside is not) causes an axisymmetric deformation mode of the film to give way to a buckled mode causing the rim to wrinkle like the edge of a leaf [19,20] as depicted by the light and dark regions around the lobes showing the film undulation (Fig. 1); the larger the drop, the larger the perimeter so that the edge of the drop is surrounded by an undulating topography with n lobes along its contact line ([9], Movie 1).

To further clarify the mechanisms at play, we turn to an even simpler realization of our observations, wherein a drop of acetone is placed on a narrow quasi-one-dimensional sagging PDMS film clamped at both ends as shown in Fig. 2(a). Now the drop spontaneously oscillates back and forth while causing the film to buckle and unbuckle ([9], Movie 8). To understand this, we note that the PDMS film underneath the drop swells due to solvent imbibition creating a local bulge due to buckling of amplitude $\sim\lambda$. This causes the acetone droplet to slide away from the swollen region, exposing the previously swollen region to the ambient atmosphere. The solvent then starts to evaporate from the swollen film, thereby regenerating it [Fig. 2(b)]. Simultaneously, the film swells at the new position of the drop causing it to buckle and pop up, causing the droplet to move back to its original position. The global sag in the PDMS strip constrains the drop to perform relaxation oscillations.

A minimal model for this represents the droplet as a particle at a scaled location $x(t)$ (made dimensionless using the drop size) in an asymmetric double-well potential $W(x, h)$ that oscillates slowly so that its minimum switches from one side to another, causing the particle to follow the minimum. The simplest form of this potential is $W(x, h) = \mu[V(x) - h(t)x]$, where $V(x) = x^4/12 - \beta x^2/2$ is associated with the double well, and the last bilinear term with a dynamically varying tilt $h(t)$ due to the simultaneous effect of (i) the location of the drop which causes the film to swell locally, and (ii) evaporation from the previous location of the drop, as shown in Fig. 2(b). There are three timescales in the problem, that associated with gravitational motion of the drop $\tau_x \sim \eta_{\text{film}}/\rho ga$, that due to swelling-induced buckling with time $\tau_s \sim \eta H^2/kE$, and evaporation $\tau_e \sim \varepsilon_b H/J$. In the simplest setting, we choose the larger of the latter two with $\tau_h = \max[\tau_s, \tau_e]$ as it defines the rate of tilting the potential, and define a ratio $\mu = \tau_h/\tau_x$. Then, in the limit of overdamped dynamics, the particle (drop) moves according to $\dot{x} = \mu[h - F(x)]$, where

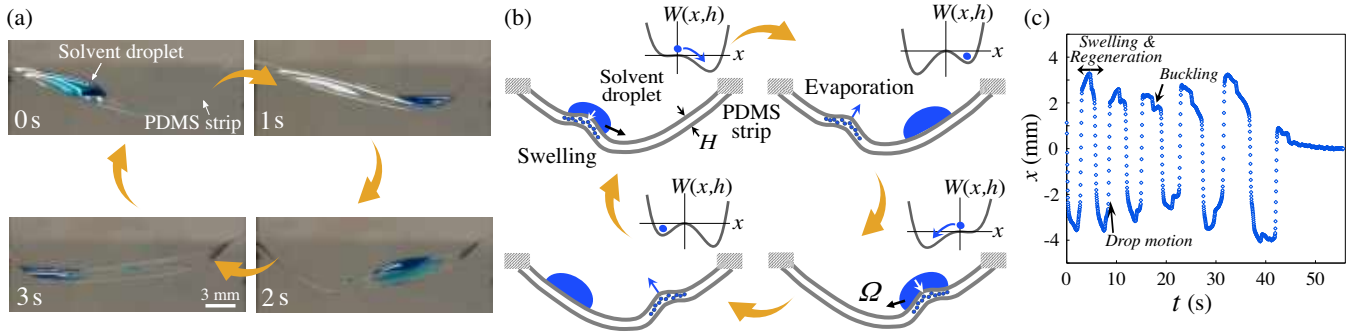

FIG. 2. 1D excitable droplet motion. (a) A drop of volume $V = 20$ μl placed on a sagging clamped PDMS strip (5 mm wide, 100 μm thick) oscillates back and forth while the film buckles periodically. (b) Schematic showing that the film locally swells in response to the solvent droplet causing the film to buckle and the droplet to slide away. The exposed swollen buckled region then loses solvent via evaporation causing the film to unbuckle. Simultaneously, the drop causes the film to swell at a new location and the process repeats. The sag in the film prevents the drop from running away and leads to an oscillating state of the drop with frequency Ω. (Inset) The shape of the potential $W(x, h)$ accompanying each film state with the droplet position $x(t)$ shown with a blue dot. (c) A trace of the x coordinate of the center of mass of an acetone droplet undergoing relaxation oscillations as a function of time, where the slow timescale is due to swelling of the PDMS film and simultaneous regeneration due to evaporation, and the fast timescale is that of the drop motion. The kinks correspond to the buckling of the film.

$F(x) = V'(x) = x^3/3 - \beta x$. Since the tilt itself evolves slowly due to evaporation from the exposed film and swelling of the film due to the droplet, we approximate this via the simple linear dynamical law $\mu\dot{h} = -x$. When $\mu \neq 0, \beta > 0$, the pair of equations is just the canonical Van der Pol equation for self-excited dynamics [21], $\ddot{x} - \mu\dot{x}(\beta - x^2) + x = 0$. For the weakly nonlinear case, when $\mu \ll 1$, we get almost periodic oscillations [9], while in the limit $\mu \gg 1$ [Fig. 2(c)], we get relaxation oscillations with slow-fast dynamics; then the drop moves quickly, with $\dot{x} \sim \mu$, but the overall tilt changes slowly with a speed $1/\mu$.

In dimensional terms, this implies that the period of the oscillations is determined by the larger of two timescales: that required to swell the film, i.e., $\tau_s \sim \eta H^2/kE$ ($\sim 1s$), until it buckles with a critical strain driven by the balance between bending and stretching [22], i.e., $\varepsilon_b \sim H/a$, and that associated with the evaporation of the drop. When the drop slides away, evaporation from the swollen bulge occurs over a timescale of $\tau_e \sim \varepsilon_b H/J$ ($\sim 5s$). Since the swelling and evaporation driven regeneration occur simultaneously, the slow timescale is of order τ_e. Over time, the drop itself shrinks due to evaporation, and the time period of oscillations increases and finally the drop stops moving when it reaches a critical size where the swelling occurs on a small enough scale that is insufficient to buckle the film ([9], Movie 8).

Having understood the basic mechanisms in the simple 1D system, we now quantify the phase space of the droplet shapes, determined by the droplet volume and the PDMS film thickness on the 2D films. On film thicknesses $H < 20$ μm, acetone droplets ($V \sim 3$–40 μL) form n-lobed chiral shapes that spin spontaneously [Fig. 3(a)]. On thicker films ($H > 40$ μm), small and large drops form spherical caps that stay pinned. The tendency for the droplet to break symmetry and move, can be parameterized by the ratio of drop size a to the elastocapillary length $\ell = \sqrt{EH^3/T}$, which characterizes the substrate softness (in terms of the tension $T \sim EH\varepsilon_{\text{cap}}$, where ε_{cap} is the elastic strain in the film due to wetting of the drop). This is denoted by the elastocapillary number $a/\ell \sim \sqrt{\varepsilon_{\text{cap}}}/\varepsilon_b$, where ε_b is the buckling strain. The shape of the lobed drops can be quantified using a simple polar representation [23] with coordinates $[r(s), \theta(s)]$ in the domain $s \in [-\pi, \pi]$, where $r(s) = a[1 + b\cos(ns)]$ and $\theta(s) = s + (c/n)\cos(ns + \psi) + \phi$. Here, a represents the overall radius of the drop, b represents the nondimensional amplitude of the lobes, c defines the asymmetry of the lobes, ψ accounts for the local phase shift at the lobes and ϕ accounts for the global phase shift [Fig. 3(b) inset; [9]]. The shape of the droplets are similar to those of cell fragments and primitive cells [15]—hardly surprising as the first few unstable modes of active drops always take the same geometric forms.

Plotting the number of lobes (n) of the experimentally observed shapes as a function of the elastocapillary number reveals that when $\sqrt{\varepsilon_{\text{cap}}}/\varepsilon_b \geq 3$, i.e., when the drop is "soft" enough, its contact line becomes asymmetric and forms lobes [Fig. 3(b)]. As the drop settles on the soft sheet with an undulating rim, the film swells and buckles to form saddle-like structures that then become asymmetric (and chiral) around the rim [Fig. 3(a)], and start to spin in a coordinated way. When $n < 6$, they synchronize and rotate, while when $n > 7$, the lobes fail to synchronize, and quiver instead ([9], Movie 9). Introducing neutrally buoyant hollow glass spheres in the droplet shows that the particles only move in a boundary layer near the contact line when $n \in [2, 6]$ ([9], Movie 10), whereas for drops with $n \sim 1$, particles move with the liquid showing global rotation of

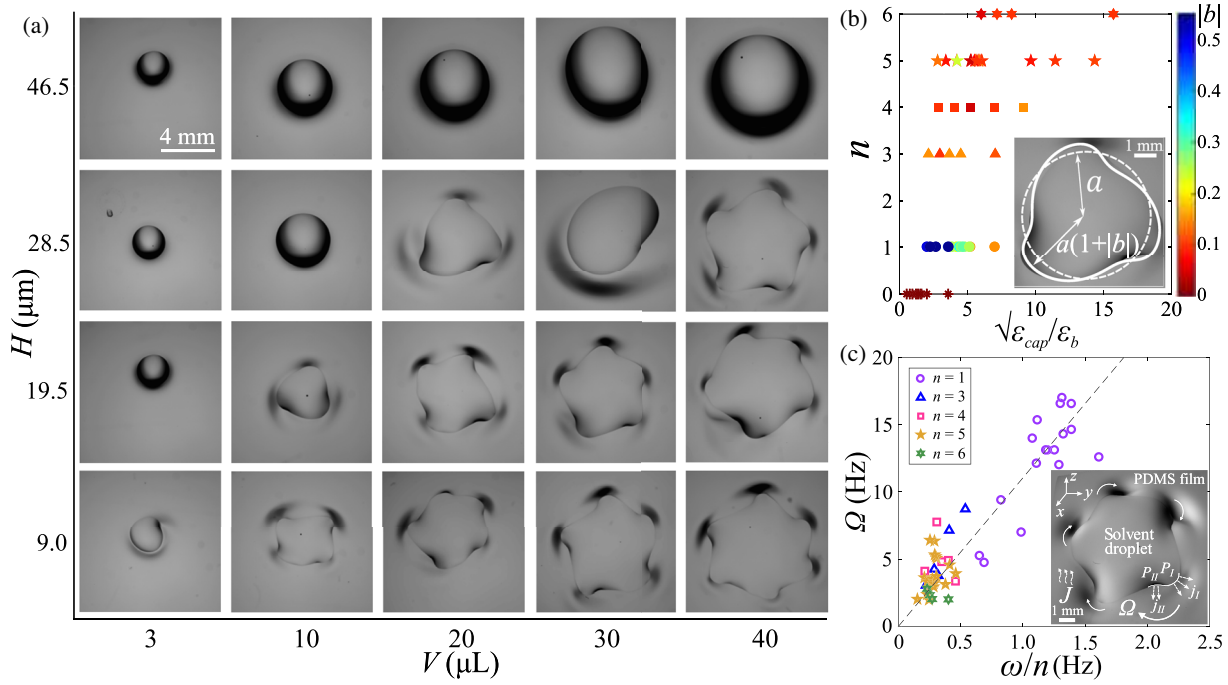

FIG. 3. (a) Phase space of instantaneous snapshots of droplets of acetone (volume V) when they are deposited on PDMS films (thickness H). Smaller droplets on thicker films are "pinned" in spherical cap state whereas larger droplets on thinner films spontaneously form lobes n (= 1 to 6) that undergo rotation. (b) Bifurcation diagram of the shapes comprising spherical pinned state ($*$) with $n = 0$ and chiral spinning state depicting number of lobes n as a function of the dimensionless elastocapillary number ($\sqrt{\varepsilon_{\rm cap}}/\varepsilon_b$). The color of each filled symbol depicts the amplitude of the lobes normalized by the radius of the drops ($|b|$). There is a critical threshold around $\sqrt{\varepsilon_{\rm cap}}/\varepsilon_b \simeq 3$ where the shapes bifurcate from spherical cap to lobed state. (Inset) An example of a fitted shape ($n = 3$) with contact radius a and amplitude $|b|$ labeled. (c) Frequency (Ω) of the spinning drops in the 3D case scales as ω/n, where $\omega \sim 1/\sqrt{\tau_x \tau_s}$, where the black dotted line is a least squares fit to the data with slope 11 (Inset). Schematic of the solvent droplet ($n = 5$) that swells the PDMS film leading to undulations, which are enhanced here for visualization, and J is the evaporative flux from the film. The liquid in the lobes traverse from hills to valleys along the circumference, giving rise to coordinated spinning of the drop with frequency Ω.

the drop. Near the contact line, variations in solvent vapor concentration from both the wetted film and the drop can lead to gradients that can cause the lobes of the droplet to break symmetry and become chiral. In all the experiments, the chirality and direction of motion of each lobe are correlated: the liquid moves from the convex side of the lobe towards its concave side ([9], Movies 1,4). To understand why this is so, we recall the Kelvin relation [24] that suggests it is easier to evaporate from convex surfaces than from concave surfaces as the vapor pressure due to positive curvature (P_I) is higher than that due to negative curvature (P_{II}). For the chiral lobes observed in our system, this would imply asymmetric evaporation from the convex and concave sides of the lobe, leading to motion from the high evaporation (convex) to the low evaporation (concave) ($j_I > j_{II}$), provided the contact line is mobile [25] [Fig. 3(c), inset]. Since the contact line of the droplet in our system sits on a saturated film, it is minimally pinned. Together, the asymmetric evaporation and the synchronized motion of lobes from convex to concave sides of the lobes give rise to an overall rotation of the drops on the PDMS film.

To understand how to generalize our understanding of the 1D oscillations of the drop to the 2D spinning drop, we note that along the rim of the drop strong gradients in swelling cause sheet to form localized wrinkles that create a periodic undulatory landscape near the rim. Spatial variations in liquid evaporation from the lobes as well as the wetted film around the drop can spontaneously break chiral symmetry of the lobes causing the rim of the drop to move tangentially—which then drives the wrinkles to rearrange via evaporation and swelling. If the number of lobes is small, the dynamics of the liquid in the vicinity of the contact line is analogous to the 1D system, except that it is periodic. If the number of lobes is large, it becomes hard to coordinate the motion of the droplet edge, leading to a shivering frustrated drop ([9], Movie 9).

Quantitatively, the frequency of a complete rotation in the periodic case for small values of μ, $\Omega \sim 1/n\sqrt{\tau_s \tau_x}$, where the liquid moves from one lobe to the next. We find that our experiments are consistent with this simple scaling law, as shown in Fig. 3(c) where the angular frequency of the droplets with varying lobe numbers collapses for the relationship $\Omega \sim \omega/n$, where $\omega \sim 1/\sqrt{\tau_s \tau_x}$ is the

characteristic frequency. In any single experiment, the drop continues to spin until its size reduces below a critical threshold determined by the parameter $\sqrt{\varepsilon_{\mathrm{cap}}}/\varepsilon_b \sim 1.8$ in Movie 2 [9], a value close to the threshold observed in Fig. 3(b).

Our experiments have shown that a volatile drop on a soft responsive substrate can create and respond to local deformation and evaporation gradients and lead to spontaneous oscillations. Three nonequilibrium processes: evaporation, solvent flow and solvent-driven swelling of a thin elastic film conspire to produce the oscillations, and one might have thought that the parameter space where these work together is small. We have shown that this is not the case—a range of solvent types and droplet sizes on thin responsive substrates satisfy the conditions for the phenomena to be observable, i.e., that $\mathrm{Pe}\sim\mathcal{O}(10)$, and the substrate be easy to buckle (i.e., thin enough). Together these processes drive self-excited motion in drops over a robust range of parameters. Harnessing such instabilities and motion in thin film systems might provide a natural way to drive small-scale engines building on recent work in this domain [26–28].

We thank Manoj K. Chaudhury for fruitful discussions. This work was supported in part by the Croucher Foundation, the Harvard Quantitative Biology Initiative and the NSF-Simons Center for Mathematical and Statistical Analysis of Biology at Harvard, Grant No. 1764269 (to G. P. T. C.), and NSF DMR 14-20570 MRSEC, NSF DMR 15-33985 Biomatter and NSF CMMI 15-36616 (to L. M.)

*Corresponding author.
lmahadev@g.harvard.edu

[1] M. K. Chaudhury and G. M. Whitesides, How to make water run uphill, Science **256**, 1539 (1992).
[2] J. Brzoska, F. Brochard-Wyart, and F. Rondelez, Motions of droplets on hydrophobic model surfaces induced by thermal gradients, Langmuir **9**, 2220 (1993).
[3] M. K. Chaudhury, A. Chakrabarti, and S. Daniel, Generation of motion of drops with interfacial contact, Langmuir **31**, 9266 (2015).
[4] F. D. Dos Santos and T. Ondarcuhu, Free-Running Droplets, Phys. Rev. Lett. **75**, 2972 (1995).
[5] V. Pimienta, M. Brost, N. Kovalchuk, S. Bresch, and O. Steinbock, Complex shapes and dynamics of dissolving drops of dichloromethane, Angew. Chem., Int. Ed. Engl. **50**, 10728 (2011).
[6] N. J. Cira, A. Benusiglio, and M. Prakash, Vapour-mediated sensing and motility in two-component droplets, Nature (London) **519**, 446 (2015).
[7] T. Liu, N. Nadermann, Z. He, S. H. Strogatz, C. Y. Hui, and A. Jagota, Spontaneous droplet motion on a periodically compliant substrate, Langmuir **33**, 4942 (2017).
[8] T. Sanchez, D. T. N. Chen, S. J. DeCamp, M. Heymann, and Z. Dogic, Spontaneous motion in hierarchically assembled active matter, Nature (London) **491**, 431 (2012).
[9] See the Supplemental Material at http://link.aps.org/supplemental/10.1103/PhysRevLett.124.258002 for Movies 1–10 and a file containing movie descriptions, additional details on experimental details and analysis tools, and estimations of Péclet and Marangoni numbers, which also includes Refs. [10–14].
[10] A. Chakrabarti and M. K. Chaudhury, Attraction of mesoscale objects on the surface of a thin elastic film supported on a liquid, Langmuir **31**, 1911 (2015).
[11] S. Dehaeck, A. Rednikov, and P. Colinet, Vapor-based interferometric measurement of local evaporation rate and interfacial temperature of evaporating droplets, Langmuir **30**, 2002 (2014).
[12] E. Y. Gatapova, A. M. Shonina, A. I. Safonov, V. S. Sulyaeva, and O. A. Kabov, Evaporation dynamics of a sessile droplet on glass surfaces with fluoropolymer coatings: focusing on the final stage of thin droplet evaporation, Soft Matter **14**, 1811 (2018).
[13] H. Sadafi, S. Dehaeck, A. Rednikov, and P. Colinet, Vapor-mediated versus substrate-mediated interactions between volatile droplets, Langmuir **35**, 7060 (2019).
[14] D. D. Bank, Surface tension, http://www.ddbst.com/ddb.html (2019).
[15] D. Bray, *Cell Movements: From Molecules to Motility* (Garland Science, New York, 2000).
[16] P. C. Wayner, Jr., Spreading of a liquid film with a finite contact angle by the evaporation/condensation process, Langmuir **9**, 294 (1993).
[17] P. J. Flory, *Principles of Polymer Chemistry* (Cornell University Press, Ithaca, NY, 1953).
[18] E. Favre, Swelling of crosslinked polydimethylsiloxane networks by pure solvents: Influence of temperature, Eur. Polym. J. **32**, 1183 (1996).
[19] H. Liang and L. Mahadevan, The shape of a long leaf, Proc. Natl. Acad. Sci. U.S.A. **106**, 22049 (2009).
[20] D. P. Holmes, M. Roché, T. Sinha, and H. A. Stone, Bending and twisting of soft materials by non-homogenous swelling, Soft Matter **7**, 5188 (2011).
[21] B. Van der Pol, On "relaxation-oscillations", Lond. Edinb. Dubl. Phil. Mag. **2**, 978 (1926).
[22] L. Landau and E. Lifshitz, *Course of Theoretical Physics* (Pergamon Press, Oxford, 1959), Vol. 3.
[23] S. Sabrina, M. Tasinkevych, S. Ahmed, A. M. Brooks, M. Olvera de la Cruz, T. E. Mallouk, and K. J. M Bishop, Shape-directed microspinners powered by ultrasound, ACS Nano **12**, 2939 (2018).
[24] W. Thomson, On the equilibrium of vapour at a curved surface of liquid, Proc. R. Soc. Edinb. **7**, 63 (1872).
[25] X. Man and M. Doi, Vapor-Induced Motion of Liquid Droplets on an Inert Substrate, Phys. Rev. Lett. **119**, 044502 (2017).
[26] M. Ma, L. Guo, D. G. Anderson, and R. Langer, Bio-inspired polymer composite actuator and generator driven by water gradients, Science **339**, 186 (2013).
[27] J. Y. Chung, H. King, and L. Mahadevan, Evaporative microclimate driven hygrometers and hygromotors, Europhys. Lett. **107**, 64002 (2014).
[28] X. Chen, L. Mahadevan, A. Driks, and O. Sahin, Bacillus spores as building blocks for stimuli-responsive materials and nanogenerators, Nat. Nanotechnol. **9**, 137 (2014).

Supplemental Information for "Self-excited motions of volatile drops on swellable sheets"

Aditi Chakrabarti, Gary P. T. Choi, L. Mahadevan

S1 Movie Captions

Movie 1: Spinning of acetone droplets on swellable PDMS film
On a PDMS film ($H = 9$ μm) afloat aqueous glycerol (50% by volume glycerol in water), acetone droplets with initial volumes $V = 3, 5$ μL form bean shapes with $n = 1$ that spin. Larger drops with initial volumes $V = 10, 40$ μL form multilobed shapes with $n = 5$ and 6 respectively. The clips are in real time. Scale bar denotes 1mm, for all movies.

Movie 2: Keratocyte-like motility of acetone drop on thicker PDMS film
On a PDMS film ($H = 28.5$ μm) afloat aqueous glycerol (50% by volume glycerol in water), an acetone drop with initial volume $V = 30$ μL undergoes oscillatory to and fro motion resembling motility of a keratocyte (skin cell), which is also in realtime.

Movie 3: Cellular migration like motility of acetone droplets on PDMS films
On PDMS films (left: $H = 9$ μm and right: $H = 28.5$ μm) afloat aqueous glycerol (50% by volume glycerol in water), acetone droplets with initial volume $V = 40$ μL form multi-lobes towards later times due to swelling gradients that lead to their

migration-like behavior. Both movies are at 2X speed.

Movie 4: Pulsatile motility visualized at high speed
On a PDMS film ($H = 19.5$ μm) afloat aqueous glycerol (50% by volume glycerol in water), an acetone drop with initial volume $V = 30$ μL undergoes pulsatile, stick-slip motion at the boundary. The movie is played at 0.1X realtime speed, i.e., it is slowed down 10 times to visualize the jumps in the motion of the lobes while they spin. Scale bar denotes 1mm.

Movie 5: Acetone drop on PDMS film with cross hatching highlights swollen film around the drop
On a PDMS film ($H = 50$ μm) afloat aqueous glycerol, an acetone drop with initial volume $V = 50$ μL undergoes oscillatory to and fro motion. A copper mesh kept under the petri dish housing the experimental setup, highlights the swollen region of the film around the drop due to the distance between the grids becoming enlarged than that away from the drop. As the drop size shrinks due to evaporation, it transitions back to having a circular contact rim. The film surrounding the drop relaxes back to flat state as the imbibed solvent leaves due to evaporation.

Movies 6 and 7: Infrared imaging of acetone droplets undergoing rotation
Droplets of acetone placed on PDMS films afloat aqueous glycerol (50% by volume glycerol in water) are imaged from top using an infrared camera, which reveal that the length scale of swelling zone (R, in Movie 6) is about twice the radius (a) of the drops. The region with diameter R is cooler than the surrounding region due to evaporative cooling. Multiple droplets in Movie 7 shows that even when they are very close to each other, they do not coalesce.

Movie 8: Droplet undergoing periodic and relaxation oscillations on thin PDMS strip
The movie shows an acetone droplet (with initial volume $V = 20$ μL, dyed with

methylene blue) oscillating on a thin PDMS strip ($H = 100$ μm, width: 5 mm) clamped on two edges with a sag. Along with the movie, the mechanism of how the oscillations arise are described. The droplet eventually comes to a halt when its size decreases below a critical threshold.

Movie 9: Large drops of acetone on thin films form multiple lobes that show uncoordinated travelling waves at their contact line
On a PDMS film ($H = 12$ μm) afloat aqueous glycerol (50% by volume glycerol in water), a large acetone droplet with initial volume $V = 40$ μL form $n \sim 10$ lobes that do not undergo synchronization transition, therefore showing erratic motion. The lobes at different parts of the drop either undergo clockwise or anticlockwise rotation without any coordinated spinning. The clip is in real time.

Movie 10: Actual versus apparent rotation
(Left) An acetone droplet (initial volume, $V = 10$ μL) on PDMS film ($H = 18$ μm, afloat aqueous glycerol) undergoes actual rotation (with lobe $n = 1$) as depicted by the motion of the neutrally buoyant hollow glass microspheres that translocate with the drop. (Right) An acetone droplet (initial volume, $V = 5$ μL) on PDMS film ($H = 10.5$ μm, afloat aqueous glycerol) undergoes apparent rotation as hollow glass microspheres do not move as much as the liquid and the modes seem to undergo a coordinated traveling wave around its edges. Both movies are played at 0.5X speed.

S2 Fabrication of polydimethylsiloxane membranes afloat aqueous glycerol & droplet excitable motion experiments

The experimental setup shown in Fig. 1(a) (main text) comprised of a thin membrane made of polydimethylsiloxane (PDMS, Sylgard 184, Dow Corning) floating atop an aqueous glycerol solution and its thickness ranged in the order of tens of microns.

The preparation of these films followed a procedure reported previously [1] with some modification, which we briefly reiterate below. A solution of 50% (by volume) glycerol (Fisher Chemical) in deionized water was degassed using house vacuum and 20 ml was added to round polystyrene petri dishes (100 mm diameter). PDMS (Sylgard 184) was mixed in 10:1 ratio (base:cross-linking agent) and thoroughly degassed. Different amounts of the PDMS pregel were gently released on the liquid surface of each petri dish and the weight of the added PDMS pregel was weighed carefully. Due to a positive spreading coefficient between PDMS and aqueous glycerol, the polymer spread across the entire surface of the aqueous glycerol. The samples were kept at room temperature for 45 minutes to allow uniform spreading of the PDMS. The samples were then baked in the oven at 75°C for 2h. The thickness ($\sim$ tens of microns) of the cured films was estimated from the weight and density of the added PDMS mixture. This method of estimating the thickness of the films was verified in previous work [1]. All experiments on the fabricated PDMS films were performed within a week after sample preparation under ambient conditions of room temperature around 22°C and relative humidity around 10%. PDMS films were also prepared using the usual spin coating method where duration of spinning and speed were varied to obtain different thicknesses. The dynamics of the drop rotation on freely floating PDMS films were captured at 100 frames per second using a wide-field microscope Axiozoom V16 (Zeiss) and all image analysis were performed using either ImageJ or Matlab. Each new experiment of drop motion was performed on a fresh location on the floating PDMS membranes. Fig. S1 shows the phase space of the acetone droplets shapes, i.e. number of lobes (n) plotted as a function of the initial volume of the droplets for a wide range of thicknesses of the PDMS membrane.

For the 1D experiments, thin strips of spin coated and cured PDMS films were cut using a fine razor blade and mounted between two cover glass slips with a sag in the film and acetone droplets (colored with methylene blue) were used to study the oscillations. Fig. S2 shows a trace of the center of mass of acetone droplet ($V \sim 20$ μL) on a strip (100 μm thick and 5 mm wide) undergoing periodic oscillations in the beginning of the experiment until the trajectory resembles more like relaxation oscillations towards the later part of the experiment. The droplet comes to a halt

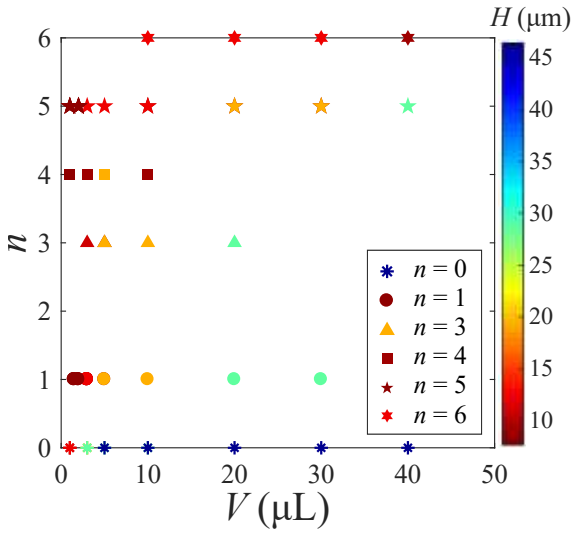

Figure S1: This plot shows the phase space of the number of lobes (n) formed on a given film thickness (H) in an acetone droplet as a function of the initial volume (V), where the color of the symbol represents the thickness of the PDMS film for the respective experiment.

when it is too small to buckle the film (Movie 8).

Varying the height of the underlying aqueous glycerol underneath the film does not affect the phenomenon of drop motion. However, if its height is reduced to less than a millimeter, the drop motion halts implying that the vertical deformations of the film in and out of plane are important for the buckling process of the membrane. In some sense, the liquid underneath provides a homing of the solvent drop and keeps it in a lower potential energy well. To check role played by the liquid underneath the film, experiments were also performed by floating the PDMS films on perfluorodecalin (Sigma Aldrich), which does not wet the PDMS film as well as does not mix with the solvents such as acetone. We observed that acetone drop underwent a few rotations after destabilizing into a multilobed shape, following which it stopped. Our experiments with the PDMS film afloat on a layer of perfluorodecalin suggests that the solvent droplet can undergo spinning for a few cycles as it would if the liquid underneath was aqueous glycerol. However, after a few cycles (over a few seconds),

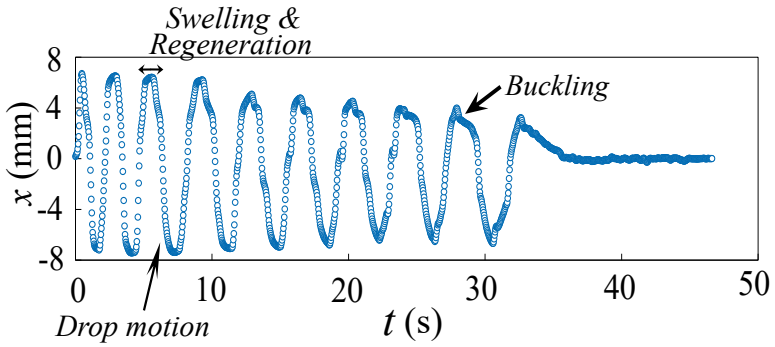

Figure S2: A trace of the x-coordinate of the center of mass of an acetone droplet undergoing periodic oscillations as a function of time, where the different timescales due to swelling of the PDMS film and simultaneous regeneration due to evaporation, and that due to drop motion are indicated. The kinks correspond to the buckling of the film.

the solvent leaving the PDMS film from below collects into a puddle between the film and perfluorodecalin since it is immiscible in perfluorodecalin. For the successful buckling of PDMS film which in turn allows the droplet to form the lobes, the film should be swollen only from one side (in our case, it is from the top, i.e., the droplet side). If there is solvent on both sides of the film (top, due to the drop, and bottom, due to acetone collecting underneath the film), this disallows buckling of PDMS film, which hinders lobe formation and thenceforth any motion. Since aqueous glycerol is miscible with the solvent (acetone in our case), it can absorb it and thereby maintain a solvent free interface between the film and the aqueous glycerol.

S3 Parametric equations for spinning droplets

Note that the shapes of the droplets in general exhibit global rotational symmetry, while the lobes of shapes are locally asymmetric. This observation motivates us to use the following parametric equations to fit each shape:

$$\begin{cases} r(s) = a(1 + b\cos(ns)), \\ \theta(s) = s + \frac{c}{n}\cos(ns + \psi) + \phi. \end{cases} \tag{S1}$$

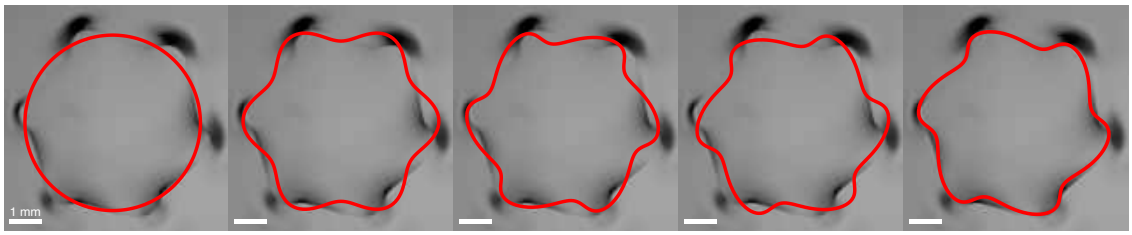

Figure S3: An illustration of the effects of the parameters a, b, c, ψ, ϕ in the parametric equation (S1). Left to right: The fit with a only (with the overall size of the shape captured), the fit with a, b only (with symmetric lobes produced), the fit with a, b, c only (with the symmetry of the lobes broken), the fit with a, b, c, ψ only (with the local phase shift corrected) and the final fit with a, b, c, ψ, ϕ (with the global phase shift corrected).

Here, $(r(s), \theta(s))$ are the polar coordinates of a point on the shape with $s \in (-\pi, \pi]$, $a > 0$ represents the radius of the shape in a global scale, b represents the amplitude of the lobes in a local scale, c accounts for the asymmetry of the lobes, $\psi \in (-\pi, \pi]$ accounts for the local phase shift at the lobes, $\phi \in (-\pi, \pi]$ accounts for the global phase shift, and n is the number of lobes (see Fig. S3 for an illustration of the effects of the parameters).

To obtain the parameters in the above parametric equations for each shape, we first set origin at the center of the shape such that it can be represented as a set of data points in the polar form $\{(r_1, \theta_1), \ldots, (r_k, \theta_k)\}$. Note that n can be obtained by directly counting the number of lobes. We then find the optimal $a, b, c, \psi, \phi, s_1, \ldots, s_k$ that yield the best fit for the following equations for all i:

$$\begin{cases} r_i = a(1 + b\cos(ns_i)), \\ \theta_i = s_i + \frac{c}{n}\cos(ns_i + \psi) + \phi, \end{cases} \tag{S2}$$

where $s_1, \ldots, s_k \in (-\pi, \pi]$. One can further simplify the above problem by combining the two equations and setting

$$s_i = \theta_i - \frac{c}{n}\cos\left[\cos^{-1}\left(\frac{\frac{r_i}{a} - 1}{b}\right) + \psi\right] - \phi, \tag{S3}$$

so that we only need to search for the best fit a, b, c, ψ, ϕ. We remark that if $n = 0$, we have a perfect circle $r = a$ and all other parameters can be omitted.

The symmetry-breaking of the droplet-film system can be parameterized by the ratio of drop size a to the elastocapillary length $\ell = \sqrt{EH^3/T}$, where T is the tension in the film ($T \sim EH\varepsilon_{cap}$, where ε_{cap} is the elastic strain in the film) denoted by the elastocapillary number $a/\ell \sim \sqrt{\varepsilon_{cap}}/\varepsilon_b$, where $\varepsilon_b \sim H/a$ is the buckling strain. The vertical component of surface tension of the droplet ($\gamma_{lv} \sin\theta_c$) can deform the thin film at the contact line due to a strain $\varepsilon_{cap} \sim \gamma_{lv} \sin\theta_c/EH$, where γ_{lv} is the surface tension of the droplet and θ_c is its contact angle with the film. Substituting for the tension gives us the scaling for the elastocapillary length, $\ell \sim \sqrt{EH^3/\gamma_{lv}}$, which has been used to calculate the $a/\ell \sim \sqrt{\varepsilon_{cap}}/\varepsilon_b$ values in Figure 3(b) in the main text.

Table S1 records the best fit parameters for some representative droplets and Fig. S4 shows the best fit parametric curves overlaid on the images of the same droplets.

S4 Péclet numbers of various solvents evaporating from PDMS films

To understand whether other solvents also show the self-generated spinning motion, we carried out experiments with fixed volume (20 μl) of various solvents such as methanol, ethanol, isopropanol, acetone, n-butanol, hexane and chloroform (Fig. S5) on varying film thicknesses. These solvents were picked such that they vary in their ability to swell PDMS [2], evaporation rates and diffusivity through the PDMS network (Table S2). Solvents such as ethanol and methanol, when deposited on the PDMS films, did not show any lobe formation and evaporated with time maintaining their spherical cap shapes. Isopropanol, n-butanol and acetone showed similar lobe formation like acetone for intermediate film thicknesses. Hexane and chloroform swelled PDMS films very rapidly and the film underwent chaotic motion. Therefore, to understand the qualitative differences between the different behaviors of the above mentioned solvents, we systematically measured the evaporative flux J (Table S2)

$H(\mu\text{m})$	$V(\mu\text{L})$	n	$a(\text{mm})$	b	c	ψ	ϕ
9.0	1	0	0.87	0	0	0	0
9.0	3	1	1.27	-0.15	0.85	2.69	0.52
9.0	3	4	1.27	0.05	0.05	-0.45	1.19
9.0	5	1	1.70	0.15	0.95	2.83	-1.05
9.0	5	3	1.70	-0.12	0.65	-0.65	0.28
9.0	5	4	1.69	0.10	-0.14	-1.18	-0.03
9.0	10	4	2.20	-0.15	0.49	-2.72	-0.07
9.0	10	5	2.33	0.08	0.00	1.57	0.13
9.0	20	5	2.77	-0.10	0.52	3.14	-0.15
9.0	30	5	3.47	-0.11	0.40	0.26	0.27
9.0	40	6	3.80	-0.10	0.16	0.21	0.00
12.0	1	0	0.75	0	0	0	0
12.0	3	5	1.27	0.08	0.22	-3.14	0.63
12.0	5	5	1.57	0.08	-0.30	-3.14	1.05
12.0	10	5	2.17	0.10	-0.40	0.2	-0.10
12.0	10	6	2.23	-0.06	-0.40	-3.14	0.02
12.0	20	6	2.67	0.10	0.50	3.14	0.23
12.0	30	6	3.07	-0.10	0.35	3.14	0.20
19.5	3	0	1.24	0	0	0	0
19.5	5	1	2.10	0.55	0.30	-0.50	0.30
19.5	5	3	2.29	0.10	0.25	1.50	0.45
19.5	5	4	2.21	0.10	0.05	0.00	0.66
19.5	10	1	3.00	0.35	-0.85	-0.15	-1.20
19.5	10	3	2.83	-0.15	-0.05	0.07	-0.15
19.5	20	5	4.05	0.10	0.40	0.00	1.45
19.5	30	5	4.62	-0.10	0.45	3.14	0.17
28.5	3	0	1.29	0	0	0	0
28.5	5	0	1.71	0	0	0	0
28.5	10	0	2.09	0	0	0	0
28.5	20	1	2.80	0.50	0.70	-0.31	0.73
28.5	20	3	2.90	0.15	0.50	0.00	0.20
28.5	30	1	3.13	-0.55	0.65	3.14	1.14
28.5	40	5	3.81	0.13	-0.60	-2.66	-0.23
46.5	5	0	1.49	0	0	0	0
46.5	10	0	2.15	0	0	0	0
46.5	20	0	2.70	0	0	0	0
46.5	30	0	3.43	0	0	0	0
46.5	40	0	3.89	0	0	0	0

Table S1: The best fit parameters a, b, c, ψ, ϕ for the parametric equation fitting the outlines of the acetone droplets. H, V, n are the film thickness, drop volume and number of lobes observed respectively.

from solvent-soaked PDMS films (area ~ 1 cm^2) by using a sensitive weighing balance that directly read how the weight of the soaked film decreased as a function of

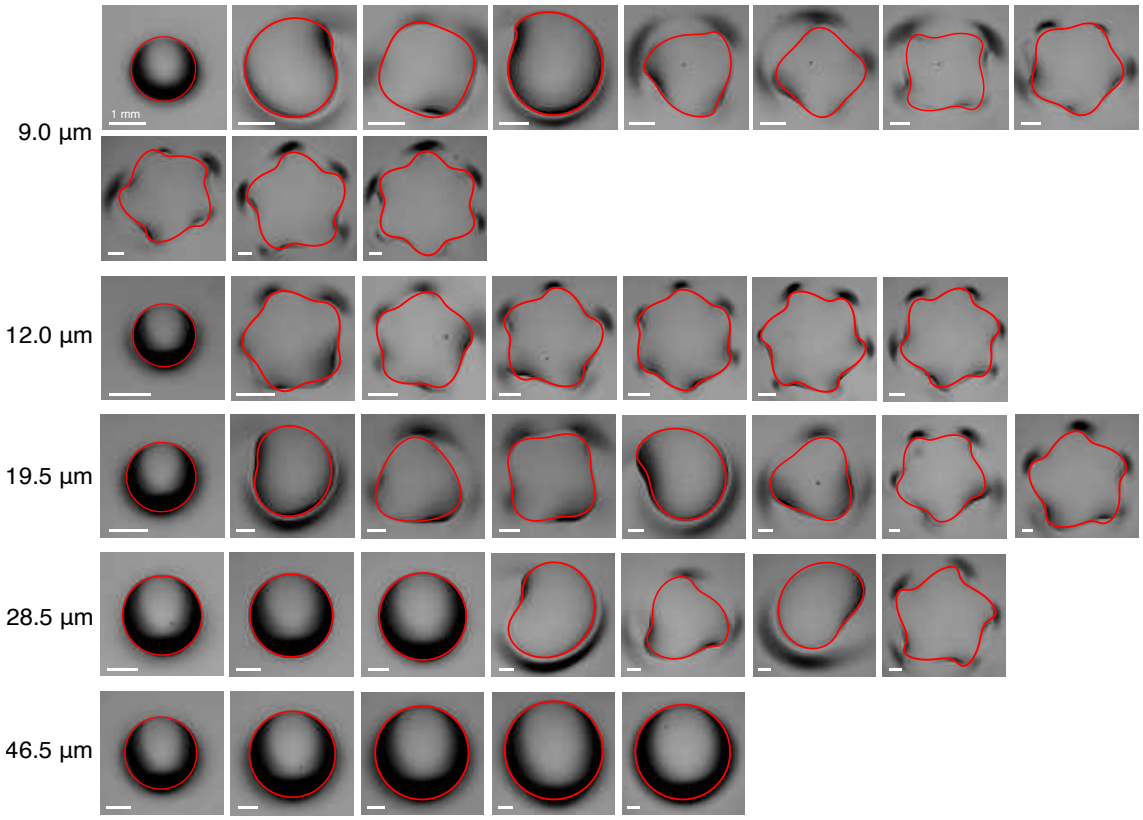

Figure S4: The best fit parametric curves overlaid on the images of the acetone droplets. The scale bar on each image represents 1mm.

time. There could be more sophisticated ways to detect vapor loss from films [3, 4, **?**] but qualitatively both the techniques will yield the same order of magnitude values for the evaporation rates. The Péclet number in each case was then determined as: $Pe \sim \eta Ja^2/kEH$. Here, k is the permeability of the drained porous PDMS network ($\sim (3K_BT/E)^{2/3} = 3.3 \times 10^{-18}$ m^2), E is the Young's modulus of PDMS (2 MPa) and η is the dynamic viscosity of each solvent. Computing the Péclet number for all solvents through the PDMS membranes, we find it to be $\mathcal{O}(10)$ where we see the spontaneous pulsatile motion, while $Pe \lesssim 10$ for all other solvents that do not show any lobe formation and spinning. A direct estimation of a PDMS film (100 μm thick) swollen with acetone drop under the microscope shows that its thickness increases

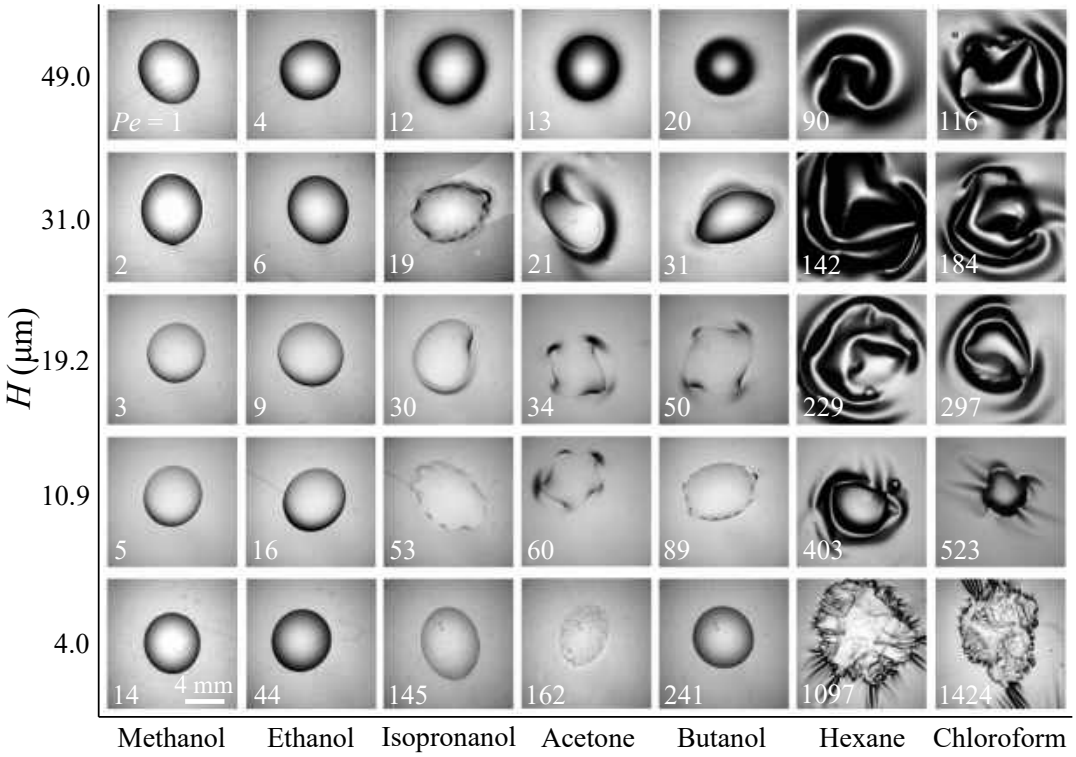

Figure S5: Snapshots of the different shapes assumed by 20 μL droplets of various solvents on different PDMS film thicknesses afloat aqueous glycerol. The respective Péclet numbers are printed in each snapshot corresponding to a specific liquid and a film thickness.

Figure S6: A PDMS film that is mounted vertically on a glass cover slip between two rigid epoxy posts swells to about 20% its original thickness when immersed in acetone (dyed with methylene blue) and reduces to its original thickness when acetone evaporates.

by approximately 20%-25% (Fig. S6).

Solvent	Density, ρ (kg/m^3)	Dynamic viscosity, η (Pa·s)	Evaporative flux measured through PDMS film, J (m/s)	Diffusivity, $D = kE/\eta$ (m^2/s)	Péclet #, $Pe = Ja^2/DH$	Swelling degree, S ([2])	Surface Tension (mN/m)
Acetone	780	3.16E-04	5.42E-07	2.09E-08	20.772	0.295	25
Butanol	810	2.80E-03	9.10E-08	2.36E-09	30.894	0.200	25
Isopropanol	786	2.04E-03	7.51E-08	3.24E-09	18.561	0.162	23
Ethanol	789	1.09E-03	4.30E-08	6.05E-09	5.683	0.063	22
Methanol	792	5.44E-04	2.70E-08	1.21E-08	1.780	-	23
Hexane	655	3.00E-04	3.86E-06	2.20E-08	140.458	-	20
Chloroform	1490	5.36E-04	2.81E-06	1.23E-08	182.264	1.530	27

Table S2: Péclet numbers and other physical properties of solvents studied on the PDMS films, estimated for $H = 20$ μm and $a = 4$ mm. The swelling degrees [2], S, for methanol and hexane are expected to be similar to ethanol and chloroform respectively.

S5 Thermal Marangoni effect in the droplets

In the following, we discuss the role of surface tension gradients in the droplet instability. As we already mentioned in the manuscript, our droplets are composed of one liquid and hence, we do not expect any compositional Marangoni effects to arise. However, thermal effects could lead to surface tension gradients as well. The thermal Marangoni number (Ma $= -\Delta\gamma L/\eta\alpha$) indicates the ratio of the thermal surface tension effects to thermal diffusion. Here, the gradient of surface tension $\Delta\gamma$ is estimated as $(\partial\gamma/\partial T)\Delta T$, where ΔT is the temperature difference across the size of the droplet L, η is the dynamic viscosity and α is the thermal diffusivity of the liquid, values of which are available in data banks [6]. If Ma$\gg$ 1, thermal surface tension gradient should drive flow within the drop and if Ma << 1, thermal diffusion should be the dominant effect. Thermal Marangoni numbers calculated for typical droplet volumes (20 μL) of the various solvents studied in our system are: Methanol, Ma=460; Acetone, Ma =1560; Butanol, Ma=101; Hexane, Ma = 1220 (Table S3). For all the calculations, ΔT was estimated from the IR movies 6 and 7 (SI) during droplet motion. In SI Fig. S5, for film thickness, H=19.2 μm, we see that methanol does not show pattern formation and sits as a hemispherical cap as it evaporates,

Solvent	Surface tension gradient $\partial\gamma/\partial T$ (mN/m.K)	Thermal diffusivity α (m^2/s)	Marangoni # Ma=$-(\partial\gamma/\partial T)\Delta TL/\eta\alpha$
Acetone	-0.13	8.3 E-08	1560
Butanol	-0.08	8 E-08	101
Methanol	-0.08	9.7 E-08	458
Hexane	-0.1	8.5 E-08	1220

Table S3: Marangoni numbers and relevant physical properties for solvents studied on the PDMS films. Values for α and $\partial\gamma/\partial T$ are obtained from Ref. [6]

acetone and butanol show 4 lobes and undergo spinning, hexane shows chaotic wrinkling and no coordinated motion. Since for all the liquids studied here, Ma$\gg$ 1, it suggests that despite having a large thermal Marangoni number, methanol, ethanol and hexane do not show the droplet instability, and are not sufficient conditions to drive the spontaneous motion as is seen in the case of acetone and butanol.

References

[1] Chakrabarti, A. & Chaudhury, M. K. Attraction of Mesoscale Objects on the Surface of a Thin Elastic Film Supported on a Liquid. *Langmuir* **31**, 1911–1920 (2015).

[2] Favre, E. Swelling of crosslinked polydimethylsiloxane networks by pure solvents: influence of temperature. *Eur. Polym. J* **32**, 1183–1188 (1996).

[3] Dehaeck, S. & Rednikov, A.& Colinet, P. Vapor-based interferometric measurement of local evaporation rate and interfacial temperature of evaporating droplets. *Langmuir* **30**, 2002–2008 (2014).

[4] Gatapova, E. Y. & Shonina, A. M.& Safonov, A. I.& Sulyaeva, V. S.& Kabov, O. A. Evaporation dynamics of a sessile droplet on glass surfaces with fluoropolymer coatings: focusing on the final stage of thin droplet evaporation. *Soft Matter* **14**, 1811–1821 (2018).

[5] Sadafi, H.& Dehaeck, S. & Rednikov, A. Vapor-Mediated versus Substrate-Mediated Interactions between Volatile Droplets. *Langmuir* **35**, 7060–7065 (2019).

[6] Dortmund Data Bank http://www.ddbst.com/ddb.html.